Journal of Power Sources 196 (2011) 1136–1140

Contents lists available at ScienceDirect

Journal of Power Sources

journal homepage: www.elsevier.com/locate/jpowsour

Short communication

Influence of microstructure of perovskite-type oxide cathodes on electrochemical performances of proton-conducting solid oxide fuel cells operated at low temperature

Makiko Asamoto, Hiroyuki Yamaura, Hidenori Yahiro*

Department of Materials Science and Biotechnology, Graduate School of Science and Engineering, Ehime University, 3 Bunkyo-cho, Matsuyama 790-8577, Japan

ARTICLE INFO

Article history:
Received 3 June 2010
Received in revised form 28 July 2010
Accepted 2 August 2010
Available online 7 August 2010

Keywords:
Cathode
Microstructure
Particle size
Proton-conducting SOFC
Perovskite-type oxide
Electrophoretic deposition

ABSTRACT

The electrochemical performances of proton-conducting SOFCs with the perovskite-type oxide cathodes were investigated at low temperature of 773 K. Among the perovskite-type oxides used in the present study, $La_{0.7}Sr_{0.3}FeO_3$ (LSF) cathode exhibited the lowest overpotential at 773 K. The power density of the SOFC was dependent on the particle size of LSF cathode. The decrease in the particle size resulted in the decrease in overpotential. The power density of the cell with LSF cathode was also dependent on the thickness of LSF cathode; in the present condition, the LSF cathode with 13-μm thickness showed the best electrochemical performance at 773 K.

1. Introduction

The doped perovskite-type oxide protonic conductors such as Yb-doped $SrCeO_3$ and Nd- or Gd-doped $BaCeO_3$ are of interest for their applications in hydrogen sensors [1], hydrogen pumps [2], membrane reactors [3], and fuel cells [4–7]. The use of proton-conducting electrolyte in solid oxide fuel cells (SOFCs) has some advantages compared with that of the oxygen ion-conducting electrolyte in SOFCs. For instance, SOFCs with proton-conducting electrolyte form water at the cathode compartment, that is, the fuel unreacted keeps pure at the anode compartment, requiring no recirculation. In addition, the activation energy of protonic conductors (0.6 eV in doped-$SrCeO_3$ [8] and 0.3–0.5 eV in doped-$BaZrO_3$ [9]) is generally lower than that of oxygen ion-conductor (0.8–1.0 eV in YSZ [10] and 0.8 eV in samarium-doped ceria [11]), indicating that ionic conductivity of former conductor becomes higher than that of the latter conductor at low temperature. In fact, the protonic conductivity of $BaCe_{0.9}Y_{0.1}O_{3-\alpha}$ was reported to be 2×10^{-3} S cm^{-1} at 673 K [12], being comparable to the oxygen ion conductivity of YSZ (1×10^{-2} S cm^{-1}) at 973 K. Accordingly proton-conducting SOFC is advantageous in low temperature use (<773 K), rather than oxygen ion-conducting SOFC.

Recently, much attention is focused on intermediate and low temperature-SOFCs (IT- and LT-SOFCs) operated at less than 1073 K because such an operation enables to use the low cost metallic interconnects and the long-term stable materials and to decrease the corrosion of components. However, the decrease in the operation temperature of a SOFC results in an increase in the overpotential of electrode, mainly cathode [13]. Therefore, the development of a superior cathode becomes an important subject to realize an IT- and LT-SOFC using proton-conducting electrolyte.

Some perovskite-type oxides, $La_{1-x}Sr_xMnO_3$ [14], $La_{1-x}Sr_xCoO_3$ [15], $La_{1-x}Sr_xFeO_3$ [16], and $La_{1-x}Sr_xCo_{1-y}Fe_yO_3$ [17], with mixed conducting property have been considered to be one of the most promising cathode materials for SOFCs with oxygen ion-conducting electrolyte. Recently, we have reported that $La_{0.7}Sr_{0.3}FeO_3$ with perovskite-type structure showed the lower cathodic overpotential than $La_{0.7}Sr_{0.3}CoO_3$, $La_{0.7}Sr_{0.3}MnO_3$, and Pt for SOFCs with proton-conducting electrolyte, $SrCe_{0.95}Yb_{0.05}O_3$ [18] and $BaCe_{0.8}Y_{0.2}O_3$ [19], at 973 K. Furthermore, we applied the electrophoretic deposition (EPD) method to fabricate the perovskite-type oxide cathode on $SrCe_{0.95}Yb_{0.05}O_3$ electrolyte surface and first reported that the electrode thickness could be exactly controlled by EPD method [20]. This result indicates that the cathodic performances of proton-conducting SOFC were strongly influenced by the microstructure

* Corresponding author. Tel.: +81 89 927 9929; fax: +81 89 927 9946.
E-mail address: hyahiro@eng.ehime-u.ac.jp (H. Yahiro).

0378-7753/$ – see front matter © 2010 Elsevier B.V. All rights reserved.
doi:10.1016/j.jpowsour.2010.08.002

of electrode. The aim of the present study is to obtain preliminary results of electrochemical performance of cathode with different particle size and thickness when proton-conducting SOFC was operated at temperature as low as 773 K. Such a low operation temperature was selected to clarify the difference in electrode ability among cathodes affecting both gas diffusion and electrocatalytically reaction although the power densities were decreased with decreasing operation temperature. The results obtained in the present study are expected to be important findings for achieving LT-SOFCs with proton-conducting electrolyte.

2. Experimental

2.1. Sample preparation

The proton-conducting electrolyte, $SrCe_{0.95}Yb_{0.05}O_3$, was prepared by a following method [18]. The mixed powders, $SrCO_3$ (Wako, 95%), CeO_2 (Wako, 99.9%), and Yb_2O_3 (Wako, 99.9%), were calcined at 1673 K for 10 h in air, uniaxially pressed into pellets under a pressure of 2000 kg cm^{-2}, and finally sintered at 1773 K for 10 h in air. The diameter and the thickness of sintered pellets were ca. 9 mm and ca. 2.3 mm, respectively.

Cathode materials, $La_{0.7}Sr_{0.3}MO_3$ (M = Mn, Fe, and Co), were prepared by the solid-state reaction. La_2O_3 (Wako, 99.99%), $SrCO_3$ (Wako, 95%), $MnCO_3$ (Wako, 99%), Fe_2O_3 (Wako, 99.5%), and Co_3O_4 (Wako, >90%) were used as starting materials. These powders were mixed in appropriate ratio and ground in a ball mill with ethanol for 24 h. After drying, the mixed powders were calcined at 1673 K for 10 h in air. The resulting powders were ground by ball-milling for 10 and 30 h to obtain homogeneous and fine particles. The particle size distribution was measured with a laser diffraction particle size analyzer (HORIBA LA-950). XRD analysis was performed to confirm the crystalline phase of samples using a Rigaku RINT2200HF diffractometer with CuKα radiation. The microstructures of cathodes were observed by a scanning electron microscope (SEM, JEOL JSL-5310).

2.2. Cathode fabrication methods

Two methods, a slurry coating method (SC method) and an electrophoretic deposition method (EPD method), were utilized for fabricating cathode on the surface of electrolyte. SC method was performed as follows. $La_{0.7}Sr_{0.3}MO_3$ oxide powders were dispersed into turpentine oil (Wako, 90%) and painted on one face of electrolyte. After drying at room temperature for several hours, the sample was heat-treated at 1173 K for 3 h to obtain good adherence between cathode and electrolyte. EPD method was performed according to the previous literature [21]. The cathode samples were added to acetylacetone containing I_2 as a charging agent and sonicated for 30 min. A constant voltage of 10–70 V was applied for 1 min between stainless electrode and electrolyte with carbon-coated surface. The thickness of electrode was controlled by changing an applied voltage. The sample was finally heat-treated at 1023 K for 3 h.

2.3. Measurement of electrochemical performance

The construction of a fuel cell was essentially the same as that reported elsewhere [18]. After Pt paste (Nilaco) was painted into one surface of electrolyte and heat-treated at 1273 K for 0.5 h in air to obtain anode, the electrolyte pellet with both electrodes was placed between silica tubes with glass gaskets to separate two compartments. A Pt wire as a reference electrode was fixed around the side of the electrolyte. After Ar gas saturated with water vapor at 298 K was supplied to the anode compartment with a flow rate of 30 cm^3 min^{-1} for 1 h, H_2 gas was supplied with a flow rate of 50 cm^3 min^{-1}. The air as an oxidant gas was supplied to the cathode compartment with a flow rate of 50 cm^3 min^{-1}. A current interruption method was employed to obtain cathodic overpotential under the operation of a fuel cell at 773 K [18].

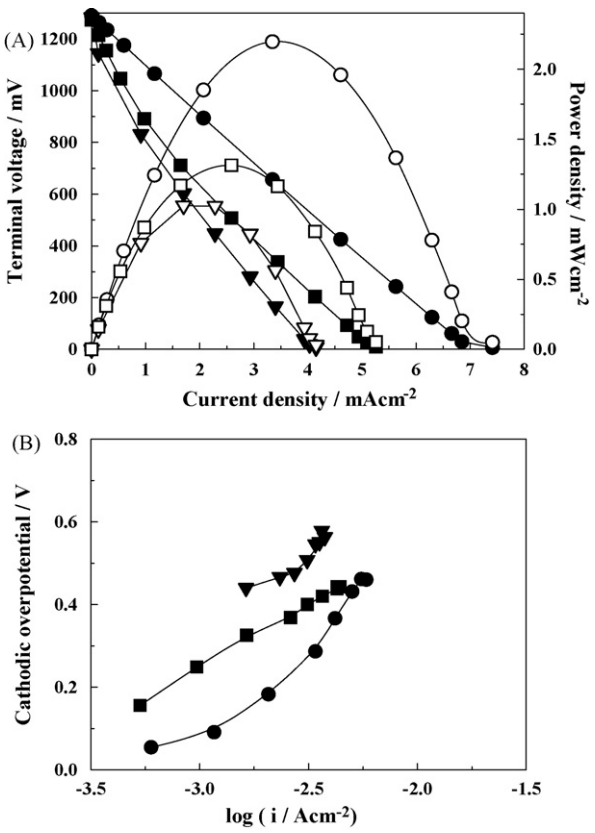

Fig. 1. (A) *I–V* (closed symbols) and *I–P* (open symbols) curves of SOFCs with (■, □) SC-LSM, (●, ○) SC-LSF, and (▼, ▽) SC-LSC cathodes at 773 K. (B) Cathodic overpotentials of (■) SC-LSM, (●) SC-LSF, and (▼) SC-LSC at 773 K.

3. Results and discussion

3.1. Electrochemical performance of perovskite-type oxide cathode

The XRD patterns of $La_{0.7}Sr_{0.3}MnO_3$ (LSM), $La_{0.7}Sr_{0.3}FeO_3$ (LSF), and $La_{0.7}Sr_{0.3}CoO_3$ (LSC) samples calcined at 1673 K provided the single phase assigned to the perovskite-type structure; no diffraction peak from a secondary phase or from the starting materials was observed. The mean diameters of LSM, LSF, and LSC particles ground by ball-milling for 30 h were estimated to be 0.4, 0.8, and 0.5 μm, respectively. These powders were utilized to elucidate cathodic performance.

Current–voltage (*I–V*) and current–power (*I–P*) curves and cathodic overpotentials for H_2–O_2 SOFCs using $La_{0.7}Sr_{0.3}MO_3$ cathodes fabricated by SC method were measured at 773 K. The results are shown in Fig. 1(A). The power densities were strongly influenced by the kind of B-site cation in perovskite-type oxide. The order of maximum power density was SC-LSF > SC-LSM > SC-LSC. Fig. 1(B) shows the cathodic overpotentials of $La_{0.7}Sr_{0.3}MO_3$ at the same temperature. The order of the cathodic overpotential was SC-LSF < SC-LSM < SC-LSC, agreeing with that of maximum power density. This suggests that the power density is dominated by the cathodic overpotential and that LSF cathode is a potential candidate for cathode material of proton-conducting SOFCs operated at low temperature.

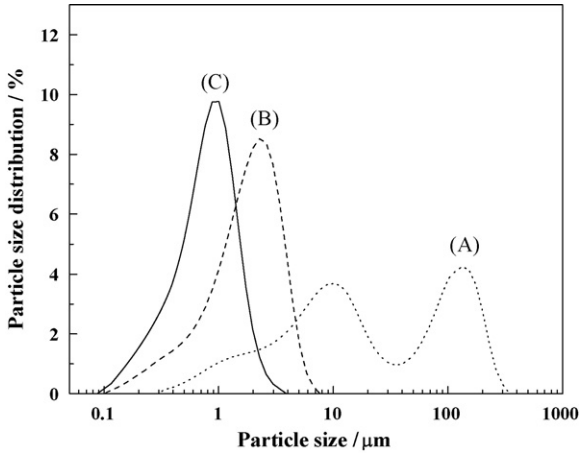

Fig. 2. Particle size distributions of LSF powders (A) as-calcined at 1673 K and ground by ball-milling for (B) 10 h and (C) 30 h.

3.2. Influence of particle size of LSF cathode on characterization and electrochemical performance

The particle size distributions of LSF powders ground by ball-milling for 10 and 30 h are given in Fig. 2, together with that of as-calcined LSF powder. The SEM photographs of the corresponding LSF powders are shown in Fig. 3. It is obvious that the LSF powders ground by ball-milling are more uniform and finer than as-calcined LSF powder. The mean diameters of LSF powders ground by ball-milling for 10 and 30 h were 1.8 and 0.8 μm, respectively. Hereafter, the LSF powders with the different particle size (A), (B), and (C), as shown in Figs. 2 and 3, are named as LSF(I), LSF(II), and LSF(III), respectively.

3.2.1. LSF cathode fabricated by SC method

Fig. 4(A) shows *I–V* and *I–P* curves of SOFCs with SC-LSF(I), SC-LSF(II), and SC-LSF(III) cathodes fabricated by SC method. The power density depended on particle size of LSF cathode; the order of maximum power density was SC-LSF(I) < SC-LSF(II) < SC-LSF(III). The cathodic overpotentials of SC-LSF (I)-(III) are depicted in Fig. 4(B). The overpotential decreased in the following order: SC-LSF(I) > SC-LSF(II) > SC-LSF(III); the lowest overpotential was achieved for the SC-LSF(III) cathode. This order in overpotential may correspond to that of the length of three phase boundary (TPB), that is, it is expected that the decrease in the particle size results in the increase in the TPB length. A similar conclusion was reported for La(Sr)Co(Fe)O_3 cathode in oxygen ion-conducting SOFC [22].

3.2.2. LSF cathode fabricated by EPD method

Fig. 5 shows SEM photographs of EPD-LSF(II) and EPD-LSF(III) cathodes heat-treated at 1023 K. The electrode powder was homogeneously deposited along the electrolyte surface regardless of surface roughness. As can be seen in Fig. 5, EPD-LSF(II) cathode made from large powders with the mean diameter of 1.8 μm was more porous than EPD-LSF(III) cathode from small powders with that of 0.8 μm.

Fig. 6(A) shows *I–V* and *I–P* curves of SOFC with EPD-LSF(II) and EPD-LSF(III) cathodes. The thicknesses of EPD-LSF(II) and EPD-LSF(III) cathodes were 16 and 13 μm, respectively, as shown in Fig. 5. The cell with EPD-LSF(III) cathode exhibited higher power density than that with EPD-LSF(II) cathode. The cathodic overpotential of EPD-LSF(III) cathode was slightly lower than that of EPD-LSF(II) cathode, as shown in Fig. 6(B). The similar result was also obtained for the LSF cathode fabricated by SC method as mentioned above. Thus, it found that the cathode with smaller particle size shows a superior performance regardless of fabrication method.

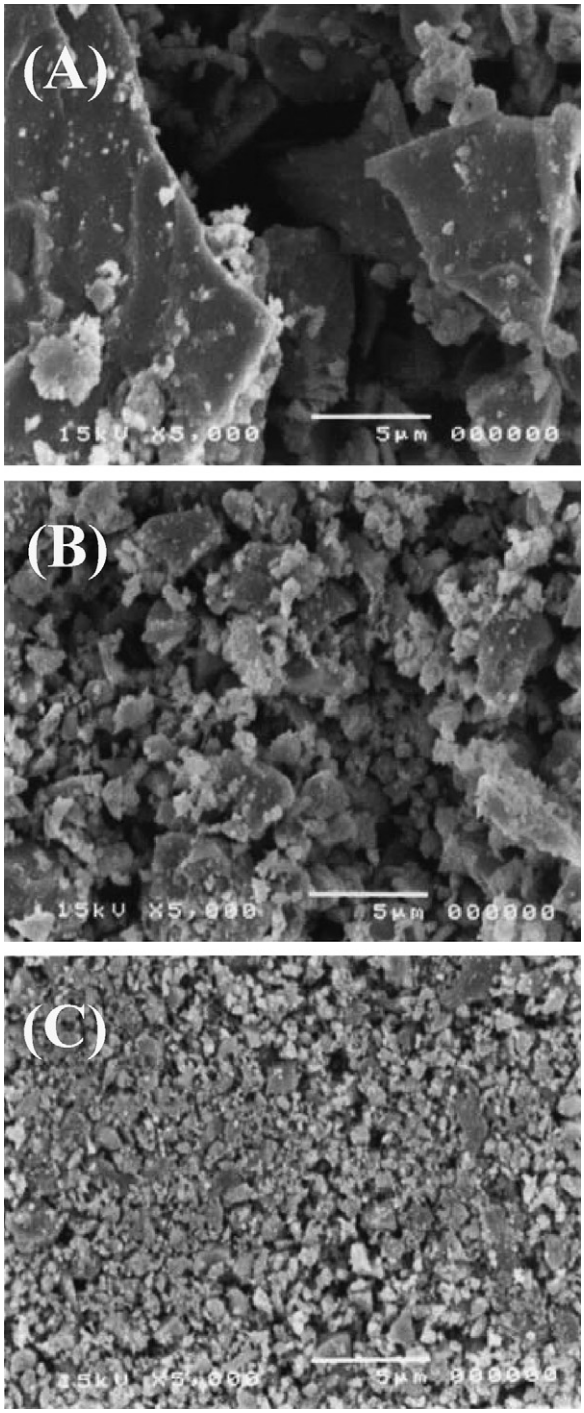

Fig. 3. SEM photographs of LSF powders (A) as-calcined at 1673 K and ground by ball-milling for (B) 10 h and (C) 30 h.

The relationship between the electrochemical performance and particle size on LSF cathode will be discussed briefly. The particle size of LSF(III) was smaller than that of LSF(II). Therefore, it is considered that the effective reaction zone (the density of the TPB) on LSF(III) cathode is larger than that on LSF(II) cathode. On the other hand, the diffusion of oxygen supplied and/or water produced in LSF(II) cathode may be easier than that in LSF(III) cathode because the former cathode was more porous than the latter one.

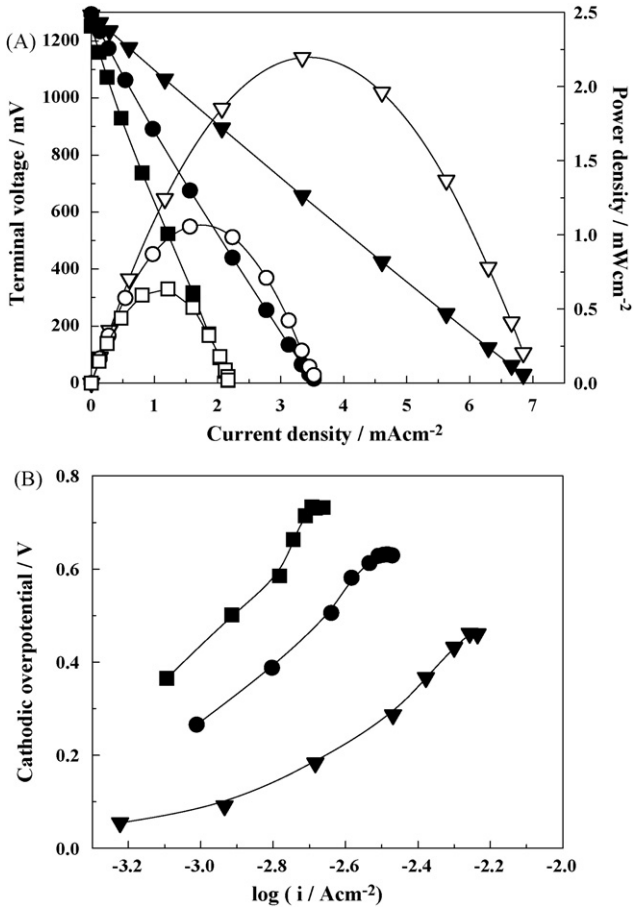

Fig. 4. (A) *I–V* (closed symbols) and *I–P* (open symbols) curves of SOFCs with (■, □) SC-LSF(I), (●, ○) SC-LSF(II), and (▼, ▽) SC-LSF(III) cathodes at 773 K. (B) Cathodic overpotentials of (■) SC-LSF(I), (●) SC-LSF(II), and (▼) SC-LSF(III) at 773 K.

Considering that LSF(III) cathode fabricated by both SC and EPD methods exhibited better performance than LSF(II) cathode, the TPB length is considered to be more important than gas diffusion for the cathode performance of proton-conducting SOFCs within the present experimental condition.

3.3. Influence of cathode thickness on electrochemical performance of SOFC

The dependence of cathode thickness on electrochemical performance was investigated for SOFCs with LSF cathode fabricated by EPD method. Fig. 7(A) shows the *I–V* and *I–P* curves of SOFCs with the EPD-LSF(III) cathodes with different thickness (4.5–31 μm). As can be seen in Fig. 7(A), the highest power density was obtained for the cell with 13 μm of cathode thickness. This optimum thickness approximately agreed with the effective thickness of cathode (<20 μm) of SOFC with oxide ion conductor [23].

The overpotentials of EPD-LSF(III) cathodes with different thickness are shown in Fig. 7(B). The cathodic overpotential monotonously increased with increasing cathode thickness. Therefore, the appearance of maximal value of power density as a function of cathode thickness cannot be explained by only cathodic overpotential. One plausible explanation is that high ohmic resistance of electrode parallel to electrolyte surface, that is, the low current collection, is a dominant factor determining electrochemical performance for a thin electrode layer. Such an ohmic resistance decreases with increasing thickness of cathode. Therefore, it was concluded that the power density was influenced by

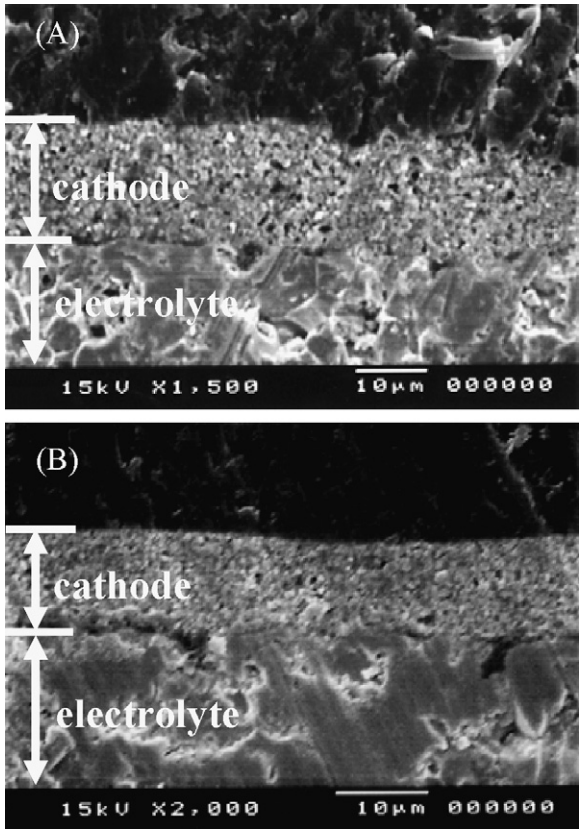

Fig. 5. SEM photographs of (A) EPD-LSF(II) and (B) EPD-LSF(III) cathodes.

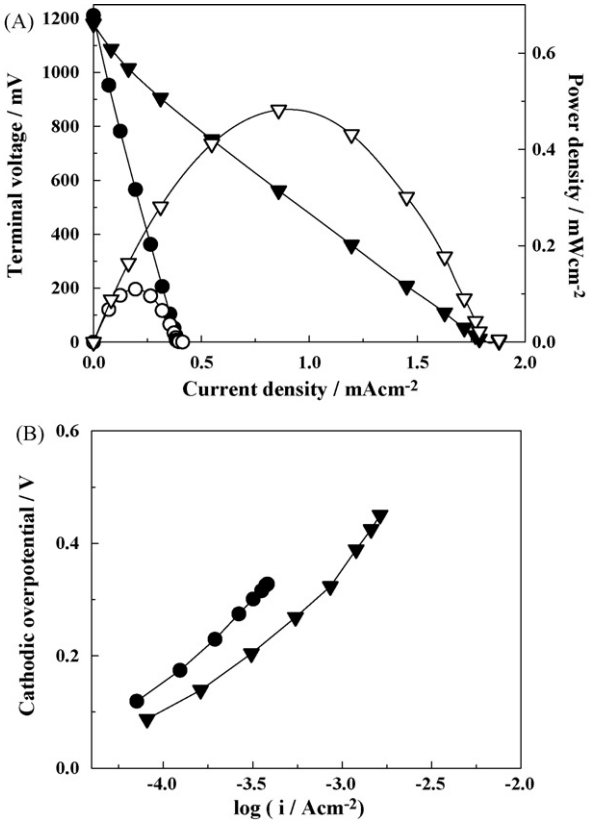

Fig. 6. (A) *I–V* (closed symbols) and *I–P* (open symbols) curves of SOFCs with (●, ○) EPD-LSF(II) and (▼, ▽) EPD-LSF(III) cathodes at 773 K. (B) Cathodic overpotentials of (●) EPD-LSF(II) and (▼) EPD-LSF(III) at 773 K.

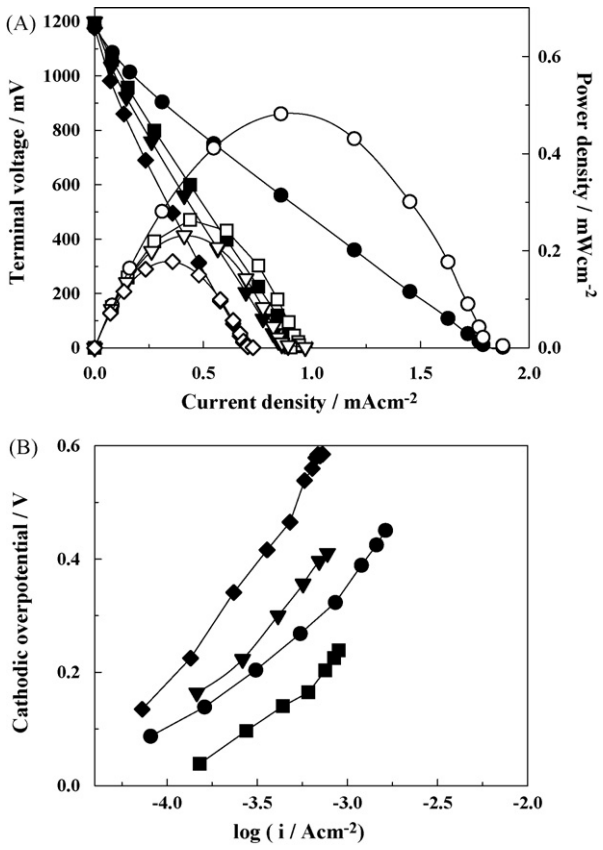

Fig. 7. (A) *I–V* (closed symbols) and *I–P* (open symbols) curves of SOFCs with EPD-LSF(III) cathodes with different thickness; (■, □) 4.5, (●, ○) 13, (▼, ▽) 21, and (◊, ♦) 31 μm. (B) Cathodic overpotentials of EPD-LSF(III) with different thickness (■) 4.5, (●) 13, (▼) 21, and (♦) 31 μm at 773 K.

both ohmic resistance of cathode and cathodic overpotential for proton-conducting SOFC at 773 K.

4. Conclusion

The electrochemical performances of the perovskite-type oxide cathodes fabricated by SC and EPD methods with uniform particles were investigated in proton-conducting SOFC at 773 K. When LSM, LSC, and LSF electrodes fabricated by SC method were used as a cathode material, the overpotential decreased in the following order: LSC > LSM > LSF at 773 K. The good performance of LSF cathode fabricated by SC method was pronounced at lower temperature.

The electrochemical performances of the LSF cathodes fabricated by EPD method were investigated in a SOFC using proton conductor. It was found that the EPD method provided uniform layer of LSF cathode with constant thickness. The overpotentials of LSF cathode were influenced by the particle size of electrode; the decrease in the particle size resulted in the decrease in the overpotential. The power density of the cell with LSF cathode was dependent on the thickness of LSF cathode fabricated by EPD method; in the present condition, the LSF cathode with 13-μm thickness showed the best electrochemical performance at 773 K.

Acknowledgement

This study was partly supported by NISSAN Science Foundation.

References

[1] N. Kurita, K. Otsuka, N. Fukatsu, T. Ohnishi, Solid State Ionics 79 (1995) 358–365.
[2] H. Iwahara, Solid State Ionics 125 (1) (1999) 271–278.
[3] S. Hamakawa, T. Hibino, H. Iwahara, J. Electrochem. Soc. 141 (7) (1994) 1720–1725.
[4] H. Iwahara, H. Uchida, M. Maeda, J. Power Sources 7 (3) (1982) 293–301.
[5] H. Iwahara, H. Uchida, S. Tanaka, Solid State Ionics 9/10 (2) (1983) 1021–1025.
[6] H. Iwahara, T. Yajima, T. Hibino, H. Ushida, J. Electrochem. Soc. 140 (6) (1993) 1687–1691.
[7] N. Bonanos, B. Ellis, M.N. Mahmood, Solid State Ionics 44 (3–4) (1991) 305–311.
[8] T. Scherban, A.S. Nowick, Solid State Ionics 35 (1–2) (1989) 189–194.
[9] H.G. Bohn, T. Schober, J. Am. Ceram. Soc. 83 (4) (2000) 768–772.
[10] J. Liu, W. Liu, Z. Lu, L. Pei, L. Jia, L. He, W. Su, Solid State Ionics 118 (1–2) (1999) 62–67.
[11] H. Yahiro, Y. Eguchi, K. Eguchi, H. Arai, J. Appl. Electrochem. 18 (4) (1988) 527–531.
[12] H. Matsumoto, Y. Kawasaki, N. Ito, M. Enoki, T. Ishihara, Electrochem. Solid State Lett. 10 (4) (2007) B77–B80.
[13] Y. Patcharavorachot, W. Paergjuntuek, W.S. Assabumrungrat, A. Arpornwichanop, Int. J. Hydrogen Energy 35 (9) (2010) 4301–4310.
[14] N.Q. Minh, J. Am. Ceram. Soc. 76 (3) (1993) 563–588.
[15] H. Uchida, S. Arisaka, M. Watanabe, Solid State Ionics 135 (1–4) (2000) 347–351.
[16] M.D. Anderson, J.W. Stevenson, S.P. Simner, J. Power Sources 129 (2) (2004) 188–192.
[17] A. Mai, V.A.C. Haanappel, S. Uhlenbruck, F. Tietz, D. Stöver, Solid State Ionics 176 (15–16) (2005) 1341–1350.
[18] H. Yamaura, T. Ikuta, H. Yahiro, G. Okada, Solid State Ionics 176 (3–4) (2005) 269–274.
[19] M. Asamoto, H. Shirai, H. Yamaura, H. Yahiro, J. Eur. Ceram. Soc. 27 (13–15) (2007) 4229–4232.
[20] M. Asamoto, S. Miyake, Y. Yonei, H. Yamaura, H. Yahiro, Electrochemistry 77 (2) (2009) 143–145.
[21] Y. Itagaki, F. Matsubara, M. Asamoto, H. Yamaura, H. Yahiro, Y. Sadaoka, ECS Trans. 7 (1) (2007) 1319–1325.
[22] K. Murata, T. Fukui, H. Abe, M. Naito, K. Nogi, J. Power Sources 145 (2) (2005) 257–261.
[23] H. Fukunaga, M. Ihara, K. Sakaki, K. Yamada, Solid State Ionics 86–88 (2) (1996) 1179–1185.